



**Environmental
Science**
Nano

**Biomolecular Corona Formation on CuO Nanoparticles in
Plant Xylem Fluid**

Journal:	<i>Environmental Science: Nano</i>
Manuscript ID	EN-ART-02-2021-000140
Article Type:	Paper

SCHOLARONE™
Manuscripts

1
2
3 Corona formation has been previously shown to significantly impact nanoparticle interactions with animal
4 and bacterial systems due to changes in particle surface properties. Inadvertent exposure of crop plants
5 to engineered nanoparticles and growing interest in applications of nanomaterials in agriculture
6 necessitates development of a mechanistic understanding of nanoparticle behavior within plants
7 including the acquisition of biomolecular coronas in vascular fluids (xylem and phloem). Here, we describe
8 the first study of biomolecule corona formation on nanomaterials in xylem fluid. We demonstrate that
9 corona formation alters the nanoparticle surface properties and involves specific proteins in the xylem
10 fluid. Corona acquisition on plant vascular fluids is expected to alter chemical transformations of
11 nanoparticles and their transport in plant systems.
12
13
14
15
16
17
18
19
20
21
22
23
24
25
26
27
28
29
30
31
32
33
34
35
36
37
38
39
40
41
42
43
44
45
46
47
48
49
50
51
52
53
54
55
56
57
58
59
60

Biomolecular Corona Formation on CuO Nanoparticles in Plant Xylem Fluid

Jaya R. Borgatta,^{*1} Christian A. Lochbaum,^{*1} Wade Elmer,² Jason C. White,² Joel A. Pedersen,^{*1,3} Robert J. Hamers^{*1}

¹ Department of Chemistry, University of Wisconsin–Madison, 1101 University Avenue, Madison, Wisconsin 53706, United States

² Department of Plant Pathology and Ecology, The Connecticut Agricultural Experiment Station, 123 Huntington Street, New Haven, Connecticut 06504, United States

³ Departments of Soil Science and Civil & Environmental Engineering, University of Wisconsin–Madison, 1525 Observatory Drive, Madison, Wisconsin 53706, United States

‡ Authors contributed equally

* Authors to whom correspondence should be addressed

Abstract

Biomolecular coatings (coronas) that form on nanomaterials have been widely investigated in animal and bacterial cell culture and in the extracellular and intracellular fluids of animals. Such coronas influence the distribution of nanoparticles within organisms, their uptake by cells, and their storage in intracellular compartments. Plants can be exposed to nanoparticles *via* either intentional application of nanomaterials in agriculture or inadvertently due, for example, to biosolids amendment of soils. Development of a mechanistic understanding of nanoparticle transport and fate within plants requires consideration of corona acquisition within plants, particularly within the vascular fluids (xylem, phloem) that transport nanoparticles throughout plants. Here, we examine the interactions between copper oxide (CuO) nanoparticles and pumpkin xylem fluid to understand corona formation in an important part of the plant vasculature system. We used CuO nanoparticles because they have emerged as a promising micronutrient source for the suppression of fungal diseases. The corona was composed primarily of proteins, despite the higher abundance of carbohydrates in xylem fluid. We used X-ray photoelectron spectroscopy to determine the thickness of the protein corona. Polyacrylamide gel electrophoresis revealed that protein binding to the CuO nanoparticle surface was selective; the most abundant proteins in the corona were not the most abundant ones in the xylem fluid. We used *in situ* attenuated total reflectance Fourier-transform infrared spectroscopy to show that the protein–CuO NP interactions were quasi-irreversible, while carbohydrate–CuO interactions were reversible. Corona formation is expected to influence the distribution and transformation of nanomaterials in plants.

Nano-Impact Statement

Corona formation has been previously shown to significantly impact nanoparticle interactions with animal and bacterial systems due to changes in particle surface properties. Growing interest in applications of nanomaterials in agriculture and inadvertent exposure of crop plants to engineered nanoparticles necessitates development of a mechanistic understanding of nanoparticle behavior within plants including the acquisition of biomolecular coronas in vascular fluids (xylem and phloem). Here, we describe the first study of biomolecule corona formation on nanomaterials in xylem fluid. We demonstrate that corona formation alters the nanoparticle surface properties and involves specific proteins in the xylem

fluid. Corona acquisition in plant vascular fluids is expected to alter chemical transformations of nanoparticles and their transport in plant systems.

Introduction

The interaction of nanoparticles (NPs) with bacterial and animal cells can be influenced by chemical and physical transformations of the NPs in environmental and biological media. Nanoparticle interaction with biomolecules – and subsequent formation of a surface coating of biomolecules (referred to as a biomolecular corona) – can alter the hydrodynamic and electrokinetic properties of NPs and influence their distribution within organisms, uptake by cells, and storage in intracellular compartments.¹⁻⁴ The chemical identity and presentation of corona molecules influences NP uptake by cells⁵⁻⁷ and depends on both the initial surface chemistry of the NP and the biomolecules with which the NP interacts. Serum, blood, cytosol, and cell culture medium have been investigated as sources of corona biomolecules and have been shown to alter NP charge, size, and morphology.^{3, 8-11}

Acquisition of biomolecular coronas by nanoparticles has been widely investigated in animal and bacterial cell culture and in the extracellular and intracellular fluids of animals.^{6, 10} In contrast, the formation of biomolecular coronas in plant vascular fluids (xylem, phloem) has not been previously reported. Nanoparticles have been proposed for use in agriculture to deliver nutrients, plant-protection chemicals, and nucleic acids.¹²⁻¹⁸ The nanoparticles can be applied either to the foliage or at the root. After internalization, corona formation may alter nanoparticle long range transport through the plant vascular system (xylem, phloem), crossing of cell walls or membranes, or storage.¹⁹ Two prior reports on corona formation from plant tissues focused on metabolite coronas acquired from intact plant leaves²⁰ and adsorption of biomolecules from leaf tissue extracts.²¹ Corona formation in plant vascular fluids is expected to be important as it may dictate the transformations and spatial distribution of NPs within plants. Recent studies have shown that the initial size and surface properties of NPs influence their spatial distribution within plants.²²⁻²⁶ Nanoparticle size and surface properties have been shown to influence the composition of the biomolecular corona formed in other biological matrices and are thus expected to exert similar influence on coronas acquired in plant fluids.²⁷ Biomolecular composition in the fluid has been shown to impact the formation of the nanoparticle corona.^{2, 28-30} The composition of xylem and phloem fluids differ dramatically from that of the fluids in the vascular systems of animals. Xylem and phloem fluids have a much higher abundance of carbohydrates relative to proteins.^{31, 32} Furthermore, protein abundance in xylem fluid (0.05 to 0.1 g·L⁻¹)³³ is orders of magnitude smaller than in animal circulatory fluids (2 to 60 g·L⁻¹).³⁴ An initial step in understanding corona formation in plant vascular fluids is to identify the predominant biomolecules in vascular fluids that are recruited to the nanoparticle surface.

Here, we investigated the composition of the biomolecular corona acquired by CuO NPs in pumpkin xylem fluid. We selected CuO NPs for investigation because prior studies showed that foliar application of Cu-based NPs upregulate plant defense pathways against fungal diseases, and previous studies have shown the presence of CuO NPs in xylem fluid when nanoparticles were applied at the root.^{12, 14-16, 35} We chose pumpkin as a model plant because relatively large volumes of xylem fluid can be isolated from this species, allowing multiple types of analytical measurements to be made on the same stock xylem solution. In situ attenuated total reflectance Fourier-transform infrared spectroscopy (ATR-FTIR) measurements reveal time-dependent association of carbohydrates and proteins with the CuO NP. X-ray photoelectron spectroscopy (XPS) studies confirm formation of a strongly surface-attached protein adlayer. By isolating NP-corona complexes and analyzing the proteins remaining in solution by gel electrophoresis, we find that protein binding is selective, with a subset of proteins selectively binding to

1
2
3 NP surfaces. Our results demonstrate that corona formation in a plant vascular fluid is a chemically
4 selective and dynamic process. These findings represent an initial step toward a mechanistic
5 understanding of how biomolecule-induced changes in surface properties influence NP interactions in
6 plants.
7

8 9 **Experimental**

10 **CuO nanoparticle synthesis**

11 All reagents were purchased from Millipore Sigma and used without further purification. We used a
12 microwave-assisted hydrothermal method to synthesize CuO NPs. Stock solutions of 1 M $\text{CuCl}_2 \cdot 2\text{H}_2\text{O}$ and
13 1 M $\text{LiOH} \cdot \text{H}_2\text{O}$ were prepared. A 938 μL aliquot 1 M CuCl_2 solution was diluted in 22.2 mL of ultrapure
14 water (Barnstead systems; 18 $\text{M}\Omega \cdot \text{cm}$), and 1800 μL of the 1 M LiOH solution was then rapidly injected.
15 The solution was stirred for 10 min, yielding a pH of 11.28. The reaction mixture was transferred to a
16 pressurized microwave synthesizer (CEM corporation) and heated to 160 °C for 10 min. The black NPs
17 were allowed to cool to room temperature. The NPs were isolated from the supernatant by centrifugation
18 (5 min, 4696g). The NPs were then cleaned by resuspension followed by centrifugation (10 min, 4696g);
19 this procedure was performed twice using water and once using ethanol. After isolating the pellet by
20 centrifugation, the particles were dried overnight at 30 °C under vacuum.
21
22
23
24

25 **Scanning electron microscopy**

26 The CuO NPs were suspended in ethanol to make a dilute suspension. The solution was bath sonicated for
27 approximately 10 min. The solution was drop-casted onto a conductive silicon wafer and air-dried. The
28 CuO NPs were imaged using a LEO Supra55 VP field-emission scanning electron microscope (SEM). The
29 SEM images were analyzed using ImageJ to extract information about the size and shape of the NPs; NP
30 dimensions were determined based on ImageJ measurements of 224 particles.
31
32
33

34 **Atomic force microscopy**

35 A high-grade mica substrate (Ted Pella) was freshly cleaved using double-sided tape. A dilute suspension
36 of CuO NPs in ethanol was drop-cast on the mica surface. The sample was then analyzed with a Bruker
37 Dimension Icon atomic force microscope using the tapping mode and TESPA-V2 tips. Atomic force
38 microscopy data were processed using Gwydion software. Height information was obtained by fitting the
39 region around the NP with a plane and extracting a height profile from the image.
40
41

42 **Powder X-ray diffraction**

43 Samples were prepared for powder X-ray diffraction by pressing CuO NPs into a thin layer of vacuum
44 grease on a zero-diffraction plate (MTI corporation). The diffraction pattern of the CuO NPs was
45 determined using a Bruker D8 Advanced powder diffractometer.
46
47

48 **Xylem fluid collection**

49 Pumpkins (*Cucurbita pepo* “Gladiator”) were seeded at the Lockwood farm in Hamden, CT in late June
50 2019 in a field mulched with black plastic. Fertilizer (NPK; 10-10-10) was applied before laying the plastic
51 mulch. Seven weeks after seeding, plant stems were cut with razor blades at the base, and xylem fluid
52 was collected from the cut ends with Pasteur pipettes (Figure S1). The xylem fluid was stored in glass vials
53 and immediately placed on ice until they could be frozen at -80 °C and shipped overnight to University of
54 Wisconsin – Madison on dry ice. Xylem fluid was stored at -80 °C until use. After warming, the fluid was
55
56
57
58
59
60

1
2
3 filtered through 0.22 μm syringe filters to remove particulate matter, and then partitioned into 5 mL
4 aliquots, flash-frozen in liquid nitrogen, and stored at $-80\text{ }^{\circ}\text{C}$ until use. Each aliquot of xylem fluid was
5 frozen/thawed a maximum of two times.
6

7 **Dynamic light scattering and laser Doppler electrophoresis**

8
9 Nanoparticle diffusion coefficients and electrophoretic mobilities were measured by dynamic light
10 scattering and laser Doppler electrophoresis, respectively (Malvern Zetasizer Nano ZS). Nanoparticles
11 were suspended in water or xylem fluid at a concentration of $50\text{ mg}\cdot\text{L}^{-1}$ immediately prior to
12 measurement. For measurement of NP diffusion coefficients and electrophoretic mobilities after 3 h
13 incubation, two suspensions were prepared with one measured at 0 h and one after 3 h incubation at 25
14 $^{\circ}\text{C}$. Diffusion coefficients and electrophoretic mobilities were measured for five analytical replicates of
15 each sample. The diffusion coefficient depends upon the viscosity of the solution. The viscosity of water
16 at $25\text{ }^{\circ}\text{C}$ is $8.90 \times 10^{-4}\text{ Pa}\cdot\text{s}$, and the viscosity of xylem fluid has been estimated to range between $8.90 \times$
17 $10^{-4}\text{ Pa}\cdot\text{s}$ and $1.2 \times 10^{-3}\text{ Pa}\cdot\text{s}$.³⁶ The impact of xylem fluid viscosities between $8.90 \times 10^{-4}\text{ Pa}\cdot\text{s}$ and $1.2 \times 10^{-$
18 $3\text{ Pa}\cdot\text{s}$ on the diffusion coefficient is examined in the Supplementary information.
19
20
21

22 **Biomolecular corona isolation and quantification**

23
24 Suspensions of CuO NPs ($0, 50, 500, \text{ or } 1000\text{ mg}\cdot\text{L}^{-1}$) were incubated in xylem fluid for 3 h and then
25 centrifuged (10 min, $14\text{ }000g$) to isolate the NPs with their surrounding corona into pellets, leaving non-
26 bound species in the supernatant. The CuO NP pellets were rinsed once with a volume of water equal to
27 that of the original supernatant and centrifuged again (10 min, $14\text{ }000g$). The supernatant from this rinse
28 was combined with that of the previous step, and the total amount of protein and carbohydrate in solution
29 was measured. The amount of protein and carbohydrate bound to the NP surfaces was determined by
30 resuspending CuO NP pellets in a volume of water equal to that of the original xylem fluid and measuring
31 the concentration of total protein and carbohydrate using the assays described below.
32

33 The amount of carbohydrate in supernatant and resuspended CuO NP pellet samples was
34 quantified using a phenol absorbance assay.³⁷ Briefly, $200\text{ }\mu\text{L}$ 5% w/v phenol in water solution was
35 combined with $250\text{ }\mu\text{L}$ of sample in a glass vial. One mL of 98% sulfuric acid was rapidly added, and the
36 solution was vortexed briefly. The solution was cooled for 1 h, and the absorbance at 460 nm was
37 measured using a BioTek Synergy 2 plate reader. To ensure consistency, a calibration curve was prepared
38 using glucose standards for every phenol solution (Figure S3).
39

40 The amount of protein in supernatant and resuspended CuO NP pellet samples was quantified
41 using a bicinchoninic acid assay. A PierceTM BCA Assay Kit (Thermo Scientific product number 23225) was
42 used to quantify protein content in the xylem fluid and in the supernatants. Briefly, $25\text{ }\mu\text{L}$ of sample was
43 added to $200\text{ }\mu\text{L}$ working reagent in a 96-well plate, incubated for 30 min at $60\text{ }^{\circ}\text{C}$, and the absorbance at
44 562 nm was measured using a BioTek Synergy 2 plate reader. Bovine serum albumin calibration curves
45 were prepared separately for every experiment to maximize consistency of results between replicate 96-
46 well plate incubations. (Figure S4).
47
48

49 **X-ray photoelectron spectroscopy (XPS)**

50
51 Samples for XPS were prepared by suspending CuO NPs at $50\text{ or } 1000\text{ mg}\cdot\text{L}^{-1}$ in xylem fluid with vortexing.
52 Suspensions were agitated on a Thermolyne Rotomix orbital shaker for 3 h, after which the CuO NPs were
53 isolated by centrifugation (10 min, $14\text{ }000g$). To remove loosely adsorbed molecules, the particles were
54 resuspended in ultrapure water and centrifuged again (10 min, $14\text{ }000g$). The NPs remaining after
55
56
57
58
59
60

1
2
3 supernatant removal were deposited onto a gold-coated silicon wafer and analyzed using a Thermo K
4 alpha X-ray photoelectron spectrometer. Survey spectra were collected with a pass energy of 200 eV and
5 a dwell time of 0.05 s, and averaging two scans. To analyze elements of interest, higher-resolution spectra
6 were collected for N(1s), O(1s), and C(1s) binding regions using a pass energy of 30 eV and a dwell time of
7 0.05 s, and averaging 15 scans. The spectra were analyzed using CasaXPS, and binding energies from all
8 spectra were calibrated to carbon at 284.8 eV. The composition and thickness of the NP coronas were
9 determined from an analysis of the relative abundance of these elements, and the thickness of the corona
10 was estimated from the attenuation of the underlying Cu(3p) emission by the corona. Spectra were
11 quantitatively analyzed using a graphical approach to solve the nonlinear equations, as described in the
12 SI. For each measurement reported here, three experimental replicates were performed and analyzed.
13
14
15

16 **Polyacrylamide gel electrophoresis**

17 We incubated CuO NPs (0, 50, 500, or 1000 mg·L⁻¹) in 1 mL xylem fluid for 3 h and sedimented the CuO
18 NPs from suspension by centrifugation (10 min, 14 000g). After removing the supernatant, the pellets
19 were resuspended in 1 mL of ultrapure water. The proteins in the samples were concentrated by acetone
20 precipitation. In detail, a 1 mL sample was combined with 4 mL acetone at -20 °C. The solution was
21 incubated for 60 min at -20 °C and centrifuged (10 min, 14 000g). Protein pellets were dried for 30 min
22 on the benchtop and resuspended in 200 µL ultrapure water. We performed a recovery study to assess
23 protein loss during the acetone precipitation by measuring protein concentration in xylem fluid and xylem
24 fluid after acetone precipitation with the BCA assay. No difference in total protein was observed between
25 the xylem fluid and xylem fluid after acetone precipitation ($p < 0.05$).
26
27
28

29 Proteins were fractionated on a Invitrogen NuPAGE™ 10% Bis-Tris Protein Gel (1.0 mm, 10-well;
30 Thermo Scientific product number NP0301BOX) following the manufacturer's protocol. The running
31 buffer (5 µL), reducing agent (2 µL), and sample (13 µL) were combined and incubated at 70 °C for 10 min.
32 A 15 µL aliquot of sample was added to each well. The gel was run at an applied potential of 200 V for 40
33 min and stained with a Pierce Silver Stain Kit (Thermo Scientific product number 24612). Gels were imaged
34 using a Azure 600 imaging system (Azure Biosystems). Images of the gels were analyzed using Igor Pro
35 software, using custom routines to extract intensity profiles along the separation direction and average
36 over the width of each line.
37
38

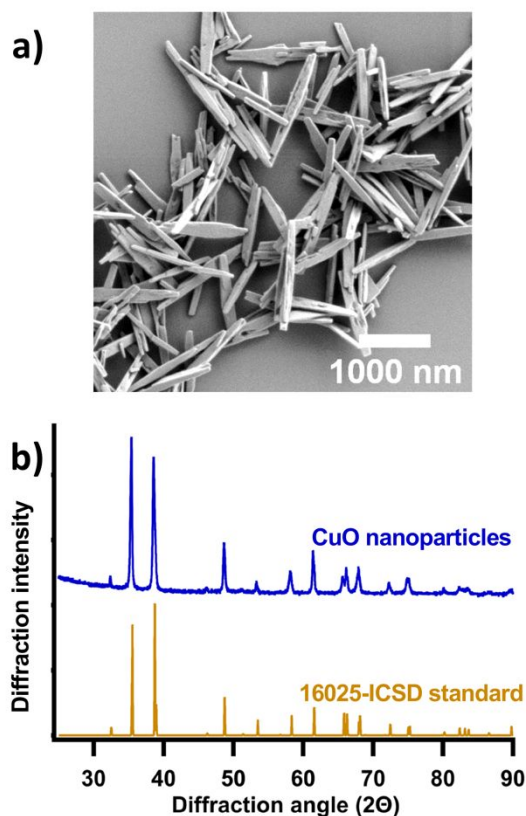
39 **Preparation of CuO nanoparticle film for *in situ* ATR-FTIR experiments**

40 The CuO film was prepared on a 10-bounce Ge trapezoidal internal reflectance element (IRE, 45° angle,
41 10 bounce, Specac gateway, Figure S4). The IRE was cleaned by exposure to UV-ozone and rinsed in
42 ethanol. The CuO NPs were suspended in 4 mL ethanol to make a 1000 mg·L⁻¹ suspension, and the
43 suspension was ultrasonicated for 10 min (repeated cycles of 10 s on, 10 s off). The suspension was drop-
44 cast in 70 µL aliquots on to the surface of the Ge IRE, and the suspension was immediately distributed by
45 spin-coating at 1000 rpm for approximately 10 s (Laurell Technologies Corporation) to produce a thin,
46 uniform layer. The process was repeated until the entire 4 mL NP suspension was deposited on the Ge IRE
47 surface. The film was annealed in a box furnace (Thermolyne) in air at 400 °C for 4 min to remove excess
48 water and to improve adhesion of the film. Scanning electron micrographs were collected to determine
49 the coverage of the CuO film on the surface of the Ge element.
50
51
52

53 ***In situ* ATR-FTIR measurements of biomolecule attachment to CuO nanoparticle surfaces**

54 To perform *in situ* ATR-FTIR measurements, the Ge IRE was mounted in a Specac Gateway flow cell
55 (internal volume 550 µL) that was then installed in a Bruker Vertex 70 FTIR spectrometer. A volumetric
56
57
58
59
60

1
2
3 flow rate of $0.5 \text{ mL}\cdot\text{min}^{-1}$ was used. Each spectrum was collected from 500 to 4000 cm^{-1} with 2 cm^{-1}
4 resolution, and 500 scans were averaged ($3.75 \text{ min}\cdot\text{scan}^{-1}$). Background scans were collected using the
5 same flow cell and ultrapure water. To collect a reference spectrum of xylem fluid, a ZnSe (45° angle, 6
6 bounce, Specac gateway, Figure S4) IRE was mounted in the flow cell, a background was collected in water,
7 and 5 mL of xylem was flowed through the system. To collect experimental data of xylem fluid
8 biomolecules interaction with the CuO NPs, the CuO-coated Ge IRE was mounted in the spectrometer.
9 Then, 5 mL of xylem fluid was flowed through the cell. The flow was stopped, and the xylem fluid
10 remaining in the ATR cell was incubated with the CuO film, for approximately 3 h. The flow was then re-
11 established using ultrapure water for 3 h to rinse away loosely adsorbed molecules. Spectra were
12 continuously recorded through the duration of the experiment (initial reference, xylem exposure, and
13 ultrapure water rinse) to monitor the temporal evolution of the protein corona. To determine the xylem
14 molecules that interact with CuO a series of model molecules were used which included malic acid,
15 dextran to represent carbohydrates, ubiquitin to represent proteins, and 1,2-dioleoyl-sn-glycero-3-
16 phosphocholine (DOPC) to represent lipids; more information is provided in the supplementary section.
17
18
19
20
21



48 **Figure 1.** Properties of as-synthesized CuO NPs: (a) scanning electron micrograph showing the morphology
49 of the CuO NPs; and (b) X-ray diffraction pattern indicating a crystal structure consistent with literature
50 data from the International Crystal Structure Database (ICSD) entry 16025 for CuO (tenorite).³⁸
51
52
53
54
55
56
57
58
59
60

Results and Discussion

Nanoparticle size, shape and crystal structure

Figure 1a shows a representative SEM micrograph of the copper oxide NPs. The NPs exhibit an anisotropic morphology and are in the form of thin, elongated sheets with lateral dimensions of 120 ± 40 nm and lengths of 900 ± 300 nm ($n=224$). The CuO NPs exhibit a powder x-ray diffraction pattern (Fig. 1b) in excellent agreement with that of a reference spectrum of CuO in the tenorite structure.³⁸ Atomic force microscopy measurements of CuO NPs deposited onto flat substrates show a typical height of approximately 50 nm (Figure S5). The anisotropic shape of the CuO NPs is consistent with the monoclinic crystal structure of tenorite and has been reported in prior studies of CuO NPs grown under conditions similar to those used here.³⁹

Nanoparticle hydrodynamic and electrokinetic properties in xylem fluid

To understand the effect of xylem fluid on hydrodynamic and electrokinetic properties of the CuO NPs, we determined the diffusion coefficients (D , from dynamic light scattering) and electrophoretic mobilities (μ_e , from laser Doppler electrophoresis) of the particles. We report D and μ_e rather than estimated hydrodynamic diameters and zeta potentials to obviate the need to invoke assumptions about particle shape, charge homogeneity, or the permeability of aggregates or biomolecular coatings. Fig. 2a shows the diffusion coefficients and electrophoretic mobilities of CuO NPs suspended in water, xylem fluid, and xylem fluid after 3 h incubation. The CuO NPs suspended in xylem fluid exhibited diffusion coefficients of $0.32 \pm 0.04 \mu\text{m}^2\cdot\text{s}^{-1}$, significantly lower than those obtained in water ($1.18 \pm 0.03 \mu\text{m}^2\cdot\text{s}^{-1}$). After 3 h incubation in xylem fluid, D decreases further to $0.17 \pm 0.03 \mu\text{m}^2\cdot\text{s}^{-1}$ ($p < 0.001$). The lower diffusion coefficient in xylem fluid cannot be attributed solely to the higher viscosity in xylem fluid relative to water. The highest reported viscosity of xylem fluid ($1.2 \times 10^{-3} \text{ Pa}\cdot\text{s}$)³⁶ does not differ enough from water ($8.90 \times 10^{-4} \text{ Pa}\cdot\text{s}$) to lead to such a dramatic decrease in diffusion coefficient (see supplementary information). The decrease in the diffusion coefficient in xylem fluid may be due to aggregation of NPs or association of xylem components with the NPs; either of these processes would be expected to increase the diffusion coefficient of the NPs.

Figure 2b shows the corresponding electrophoretic mobilities in these solutions. While CuO NPs suspended in water exhibit $\mu_e = +2.7 \pm 0.6 \text{ cm}^2\cdot\text{mV}^{-1}\cdot\text{s}^{-1}$, CuO NPs suspended in xylem fluid display a much lower mobility, $\mu_e = +0.2 \pm 0.3 \text{ cm}^2\cdot\text{mV}^{-1}\cdot\text{s}^{-1}$. Incubation for 3 h did not produce any further change in mobility ($\mu_e = +0.1 \pm 0.3 \text{ cm}^2\cdot\text{mV}^{-1}\cdot\text{s}^{-1}$; $p > 0.05$). The smaller magnitude of the electrophoretic mobility in xylem fluid vs. water may have arisen from the association of xylem fluid molecules with the surface of CuO NPs or the higher ionic strength of the xylem fluid relative to water. The ionic strength of xylem fluid has been reported to be $32 \pm 14 \text{ mM}$ (*Ricinus communis*).⁴⁰ Using this value, the difference in ionic strength between water and xylem fluid is sufficient to cause the observed decrease in electrophoretic mobility (see supplementary information). In addition to the difference in ionic strength, adsorption of molecules to the surface of CuO NPs is consistent with prior studies reporting changes in NP electrophoretic mobility due to adsorption of charged biomolecules²⁷ or small charged molecules⁴¹ which are both present in xylem fluid. Neutralization of NP surface charge by charged organic (macro)molecules in xylem fluid would be consistent with the influence of electrostatic attraction between the CuO surface and components of the xylem fluid. Neutralization of NP surface charge may also lead to loss of particle colloidal stability and help explain the decrease in observed diffusion coefficient.^{42, 43}

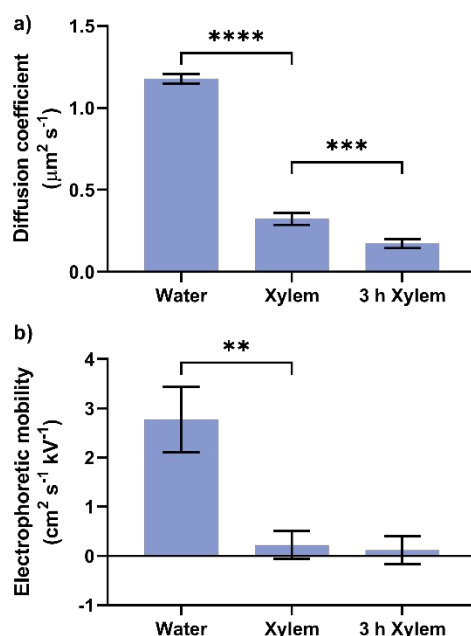


Figure 2. (a) Diffusion coefficients and (b) electrophoretic mobilities of CuO NPs are lower in xylem fluid than in water. Diffusion coefficients were determined from dynamic light scattering experiments; electrophoretic mobilities were determined by laser Doppler electrophoresis. Measurements are for $50 \text{ mg}\cdot\text{L}^{-1}$ suspensions of CuO NPs. Error bars denote one standard deviation. Notation for significance of differences: **, $p < 0.01$; ***, $p < 0.001$, ****, $p < 0.0001$.

CuO nanoparticles adsorb proteins from xylem fluid

As an initial step toward determining the composition of the biomolecular corona acquired in xylem fluid, we quantified the amount of carbohydrate and protein associated with the CuO NPs using a phenol-based total carbohydrate assay and the bicinchoninic acid (BCA) assay, respectively. We focused on proteins and carbohydrates because they have been previously reported in xylem fluid at quantifiable concentrations and because these classes of molecules have been shown to form coronas on nanoparticles.^{28, 44} Protein and carbohydrate concentration of fluid varied among plants sampled ($90 \pm 20 \text{ mg}\cdot\text{L}^{-1}$ and $250 \pm 50 \text{ mg}\cdot\text{L}^{-1}$, respectively). Differences in concentration among samples were accounted for by measuring concentrations of biomolecules for every aliquot to normalize results to starting protein and carbohydrate concentrations. We incubated CuO NPs at 0, 50, 500, and $1000 \text{ mg}\cdot\text{L}^{-1}$ in xylem fluid for 3 h, sedimented the NPs *via* centrifugation and analyzed both the supernatant and isolated CuO NPs for carbohydrate and protein content. Figure 3a shows the amount of carbohydrate remaining in the xylem fluid supernatant after exposure to the CuO NPs; incubation with CuO NPs did not result in detectable removal of carbohydrate at any NP concentration investigated relative to control samples ($p > 0.05$). Figure 3a also shows the corresponding measurements of the amount of carbohydrate extracted from the NP (“CuO-bound”). The amount of carbohydrate bound to the NPs is below our estimated limit of detection ($< 10 \text{ mg}\cdot\text{L}^{-1}$).

Figure 3b shows the concentration of protein remaining in xylem fluid supernatant after incubation with CuO NPs at three NP concentrations with the corresponding concentrations of protein

extracted from sedimented nanoparticles. We note that the total mass concentration of carbohydrates (Fig. 3a, $\sim 270 \text{ mg}\cdot\text{L}^{-1}$) is much higher than that of proteins (Fig. 3b, $\sim 80 \text{ mg}\cdot\text{L}^{-1}$). At the lowest CuO NP concentration investigated ($50 \text{ mg}\cdot\text{L}^{-1}$), protein removal from the xylem fluid was below the detection limit of the assay ($< 5 \text{ mg}\cdot\text{L}^{-1}$); furthermore, no significant protein was extracted from CuO NPs that were isolated by centrifugation. At higher CuO NP concentrations (500 and $1000 \text{ mg}\cdot\text{L}^{-1}$), significant amounts of protein were adsorbed and removed from solution ($p < 0.05$), and equivalent amounts of protein were extracted from the CuO NPs that were isolated by centrifugation. In all cases, the sum of the amount of protein in the supernatant and the amount extracted from the NPs corresponded to the original amount of protein in xylem fluid. The detection of surface-bound protein without detectable surface-bound carbohydrate from xylem fluid indicates that the biomolecular corona composition after 3 h incubation is composed primarily of protein. As the NP concentration increases, the amount of protein detected on the NPs increases as does the magnitude of the amount removed from the supernatant; this trend is consistent with the increase in surface area available for corona formation at higher nanoparticle concentrations. To investigate the relationship between CuO NP surface area and protein adsorption, we analyzed the thickness of the corona formed.

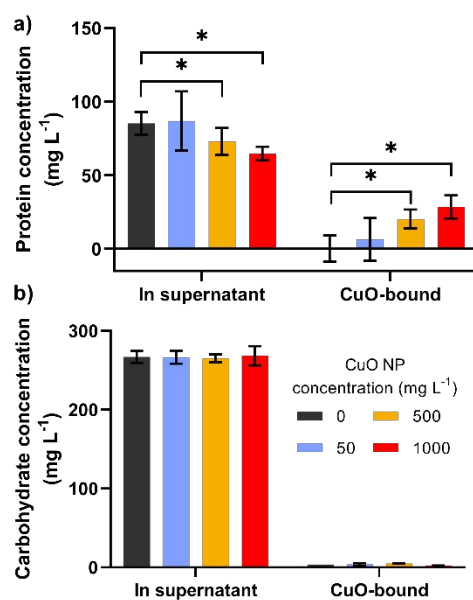


Figure 3. Concentrations of (a) carbohydrate or (b) protein remaining in supernatant and associated with CuO NPs after 3 h incubation and subsequent sedimentation at the indicated concentration of CuO NPs in xylem fluid. Carbohydrate concentration was measured by the phenol total carbohydrate assay; protein concentration was measured by the BCA assay. Error bars represent one standard deviation. Notation for significance of differences: *, $p < 0.05$.

Dependence of corona thickness on CuO nanoparticle concentration

We used X-ray photoelectron spectroscopy to directly probe the elemental composition of xylem fluid components bound to the CuO NPs as well as their chemical state. X-ray photoelectron spectroscopy is an *ex situ* method that provides quantitative information about the strongly bound corona components that persist after rinsing and drying. Therefore, XPS provides information about the hard corona and

1
2
3 associated strongly-bound molecules, while the weakly associated molecules of the soft corona were
4 likely removed before XPS analysis. Figure 4a shows survey XPS spectra of CuO NPs that had been exposed
5 to xylem fluid for 3 h. Peaks associated with C, O, and Cu are apparent in the spectra for all samples.
6 Spectra of CuO NPs that had been exposed to xylem fluid also exhibit surface nitrogen that is detectable
7 over 3σ of the noise, while no detectable nitrogen is observed in spectra from unexposed CuO samples.
8 After exposure to xylem fluid, the absolute and relative intensities of the peaks change; the absolute
9 intensities of the Cu(2p) and O(1s) peaks decrease, while C(1s) emission intensity increases and a new
10 N(1s) peak appears. The XPS data yield two complementary pieces of information. First, the attenuation
11 of the Cu(2p) and O(1s) emission by the biomolecular corona provides a way to assess the overall thickness
12 of the strongly bound corona components. Second, the relative intensities of emissions from N(1s), C(1s),
13 and O(1s) provide information about the chemical composition of the corona.

14
15
16 The thickness of the corona can be assessed from XPS measurements by quantifying the degree
17 to which the Cu(2p) emission intensity is decreased upon formation of the NP corona, or by measuring
18 the emission intensity from elements specific to the NP core (e.g., Cu) and those that are specific to the
19 corona (e.g., N). In the latter case, the corona thickness can be determined from the equation:

$$\frac{(1 - e^{-t/\lambda_{N,P}\cos\theta})}{e^{-t/\lambda_{Cu,P}\cos\theta}} = \frac{A_N \rho_{Cu,CuO} S_{Cu} \lambda_{Cu,CuO}}{A_{Cu} \rho_{N,P} S_N \lambda_{N,P}} \quad (1)$$

20
21
22 where t is the thickness of the biomolecular corona; S_{Cu} and S_N are the atomic sensitivity factors for Cu
23 and N; $\rho_{Cu,CuO}$ is the atomic number density of Cu atoms in CuO; $\lambda_{Cu,CuO}$, $\lambda_{Cu,P}$, and $\lambda_{N,P}$ are the inelastic mean
24 free paths (IMFPs) of Cu photoelectrons in CuO, Cu photoelectrons passing through the protein layer, and
25 N photoelectrons in the protein layer; and θ is the angle of collection of photoelectrons with respect to
26 the surface normal. Using estimated IMFPs, this equation can be solved to determine an approximate
27 corona thickness (see Supplementary Information). The corona thickness was also estimated in the same
28 manner using the C(1s) signal; the value presented represents an average of the corona thicknesses
29 calculated using both the C(1s) and the N(1s) data, which were similar. Using this approach, we estimated
30 corona thickness to be 5.1 ± 0.2 nm at a NP concentration of $50 \text{ mg}\cdot\text{L}^{-1}$ and 1.9 ± 0.1 nm at a NP
31 concentration of $1000 \text{ mg}\cdot\text{L}^{-1}$. We note that a 20-fold increase in NP concentration decreased the average
32 corona thickness by a factor of approximately two. Rigorously accurate determination of corona thickness
33 from XPS measurements would require inclusion of the uncertainty in the IMFP values. Although we did
34 not include the error in the IMFPs in our analysis, such errors are systematic and would not change the
35 overall conclusion that thinner coronas were found at higher NP concentrations. This observation suggests
36 that specific proteins are depleted from the xylem fluid. This conclusion is consistent with results from the
37 BCA assay (*vide infra*) showing partial removal of proteins at high NP concentrations.
38
39
40
41
42
43
44
45
46
47
48
49
50
51
52
53
54
55
56
57
58
59
60

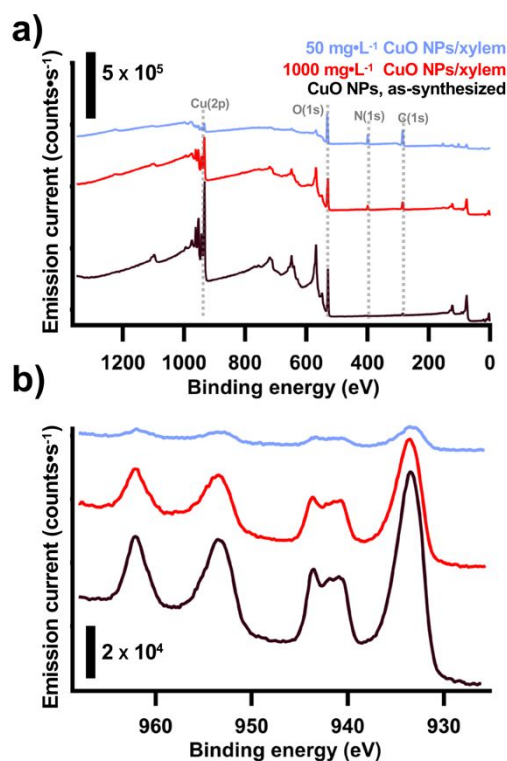


Figure 4. (a) Survey and (b) Cu(2p) X-ray photoelectron spectra from CuO NPs after interaction with xylem fluid.

To assess the consistency between the results of the XPS and protein depletion studies, we estimated the amount of protein that would be removed from the xylem to form coronas with the thicknesses estimated from XPS. We approximated the CuO NPs rectangular prisms with dimensions of 900 nm × 120 nm × 50 nm based on SEM measurements, and we approximated the corona as a layer of protein of uniform density ($1.35 \text{ g}\cdot\text{cm}^{-3}$)⁴⁵ covering the entire CuO NP surface. We estimated that formation of a 1.9 nm thick corona on CuO NPs in a 1000 mg·L⁻¹ suspension would remove 24 mg·L⁻¹ protein from the xylem fluid; this is very close to the protein removal of $28 \pm 5 \text{ mg}\cdot\text{L}^{-1}$ measured by BCA assay. We also estimated that formation of a 5.1 nm thick corona on CuO NPs in a 50 mg·L⁻¹ suspension would be accompanied by a removal of 3.2 mg·L⁻¹ protein from the xylem fluid. This value is below the BCA detection limit of 5 mg·L⁻¹ and is consistent with our inability to detect significant protein loss *via* the BCA assay at the 50 mg·L⁻¹ CuO NP concentration.

To obtain more detailed chemical information about the corona, we collected XPS spectra at higher resolution in the Cu(2p), O(1s), N(1s), and C(1s) regions. The high resolution Cu(2p) spectra in Fig. 4b show that CuO NPs exposed to water (but not xylem fluid) exhibit a 2p_{3/2} peak at a binding energy (BE) of $932.60 \pm 0.08 \text{ eV}$, a 2p_{1/2} peak at $952.60 \pm 0.08 \text{ eV}$, and shake-up features at $942.1 \pm 0.1 \text{ eV}$ and $961.90 \pm 0.03 \text{ eV}$.⁴⁶ For the 50 mg·L⁻¹ nanoparticle concentration, the Cu(2p) emission intensity (Figure 4) is attenuated by a factor of ~13 compared to bare CuO samples, but the overall shapes and relative intensities of the individual Cu peaks remain unchanged. This attenuation factor (F) is also consistent with a corona thickness of ~5 nm, as calculated using the following equation:

$$F = e^{(-\frac{t}{\lambda})} \quad (2)$$

where, t is the thickness and λ is the inelastic mean free path approximated at 2 nm. The O(1s) region displayed in Fig. 5a shows a large peak at 529.40 ± 0.04 eV from bulk CuO and a smaller peak at 530.88 ± 0.06 eV that is consistent with Cu–OH groups.⁴⁷ The peak energies for the adsorbates on CuO NPs from the $50 \text{ mg}\cdot\text{L}^{-1}$ and $1000 \text{ mg}\cdot\text{L}^{-1}$ suspensions in xylem fluid were similar; we report the binding energies for only the $50 \text{ mg}\cdot\text{L}^{-1}$ sample here. The C(1s) region shown in Fig. 5b exhibits a peak at 284.80 eV (used as our internal binding energy calibration) due to alkane-like adventitious carbon contamination, along with a smaller peak at 287.38 ± 0.04 eV; the higher BE of this peak is typical for oxidized carbon forms such as carbonyl groups. The CuO NPs that had been incubated with xylem fluid (and then rinsed) exhibit changes in the C(1s) and O(1s) peaks and show a new peak in the N(1s) region (Fig. 5c). In the O(1s) region, particles exposed to xylem fluid exhibit peak at 532.06 ± 0.03 eV that falls within the range of energies typically observed for carbonyl (C=O) oxygens in proteins.⁴⁸ This is consistent with the appearance of a peak at 288.1 eV in the C(1s) region that is consistent with C=O moieties. The C(1s) region in spectra of CuO NPs exposed to xylem fluid also contains a peak at 285.8 eV which is consistent with C–N or C–O moieties in proteins^{49, 50} and C–O–C groups in carbohydrates.⁵¹ The N(1s) region in spectra of CuO NPs exposed to xylem fluid shows a single, sharp peak at 399.9 ± 0.2 eV, similar in appearance to prior reports of the proteins fibrinogen, bovine serum albumin, and soy protein (Figure 5c).^{49, 52, 53} The binding energies of the C(1s), N(1s), and O(1s) are consistent with functional groups present in xylem fluid including proteins, carbohydrates, small organic acids, and phospholipids. However, the relative atomic abundances of C, O, and N indicate that proteins are the main biomolecules present.

The changes in surface composition can be expressed as atomic percentages, where the atomic percentage of element X is given by

$$\%x = 100 \times \frac{\frac{I_x}{\text{IMFP}_x S_x \lambda_j}}{\sum_j \left(\frac{I_j}{\text{IMFP}_j S_j \lambda_j} \right)}$$

I_j is the area of the photoemission peak for element j , IMFP_j is the inelastic mean free path for element j , S_j is the atomic sensitivity factor for element j , and λ is the inelastic mean free path at the energy of the photoelectrons for each element. The summation is over photoemission peaks from all elements corresponding to the corona layer (here, C, N, and the high binding-energy component of O). To calculate the atomic percentages in corona constituents, we use only the O(1s) peak component centered at 532.06 ± 0.03 eV that corresponds to the protein layer, thereby excluding the O(1s) signal arising from the underlying CuO.

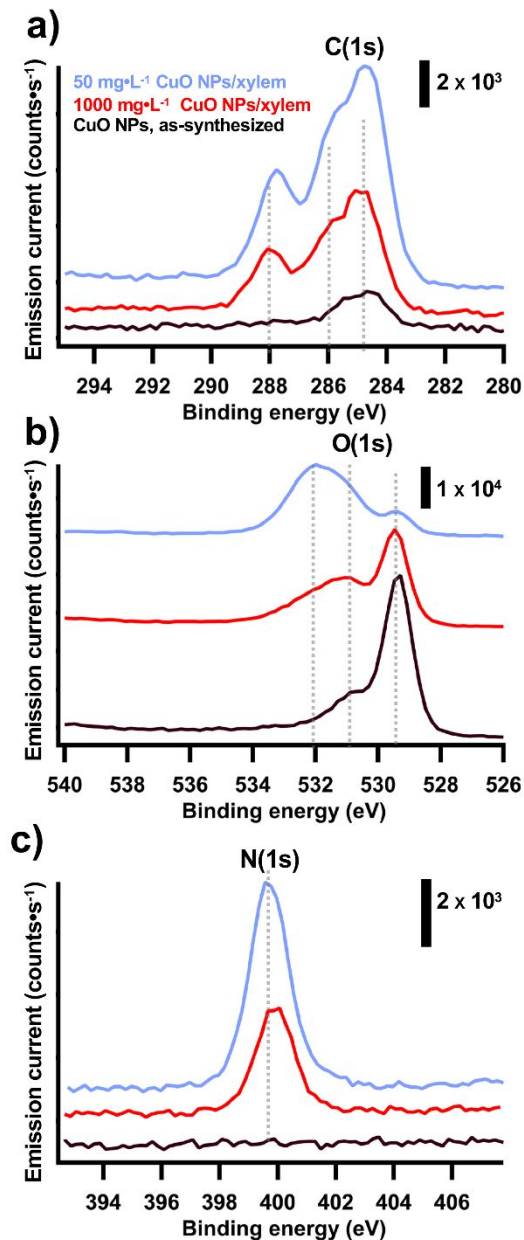


Figure 5. High resolution XPS spectra in the (a) C(1s), (b) O(1s), and N(1s) regions for CuO NPs that had been incubated with xylem fluid.

Figure 6 shows that calculated atomic abundances of C, O and N atoms in the corona layer were similar for CuO NPs that had been incubated with xylem fluid at 50 and 1000 mg·L⁻¹ concentrations. The CuO from the 1000 mg·L⁻¹ suspension exhibited atomic percentages of 45.7 ± 0.1%, 12.2 ± 0.2%, and 42.1 ± 0.2% for C, N, and O, respectively. The atomic composition of individual carbohydrates and proteins vary in accordance with their specific molecular structures. Nonetheless, their atomic compositions fall into distinct ranges. Both carbohydrates and proteins contain approximately 50% carbon, but carbohydrates contain significantly more oxygen (45-49% O vs. ~35% O for proteins) and less nitrogen (<3% vs. 15-20% N for proteins).⁵⁴ The compositions of the coronas on the CuO NPs, particularly the high N content, are similar to those of typical proteins and not consistent with typical carbohydrates. The atomic abundances

of molecules in the coronas on the CuO NPs were similar for the 50 mg·L⁻¹ and 1000 mg·L⁻¹ NP suspensions (paired t-test, $p > 0.05$), suggesting that while the corona layer has a different thickness, it is comprised of proteins in both cases. The atomic abundances of C, O, and N also suggest that very little carbohydrates or other biomolecules are found in the corona isolated after a rinsing step.

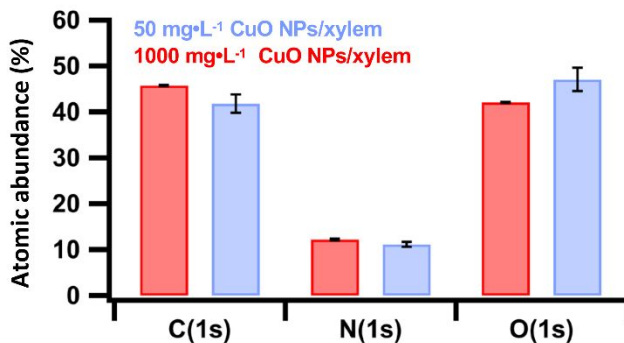


Figure 6. The atomic abundances of C, O, and N in the coronas on CuO NPs are consistent with the biomolecular corona being composed primarily of proteins. Atomic abundances are similar in elemental composition at both NP concentrations ($p > 0.05$).

In summary, the corona formed on CuO NPs from xylem fluid is thinner at the higher (1000 mg·L⁻¹) NP concentration, and atomic abundances of C, N, and O are in the range typical of proteins, for both high and low nanoparticle concentrations. Our data suggest that recruitment of proteins to the CuO surface is selective. At low NP concentrations, strongly binding proteins associate with the NP surface to form a corona with an average thickness of ~5 nm. The xylem fluid appears to contain insufficient amounts of high affinity proteins to form a similarly thick coating on the CuO NPs when the NPs are present at a 20-fold higher concentration. This is due to the larger amount of CuO surface area available to bind proteins at the higher NP concentration, leading to a thinner (~2 nm thick) corona of approximately the same composition.

Preferential binding of specific proteins to CuO NPs

To confirm that specific proteins from xylem fluid selectively bind to CuO NPs, we examined the proteins remaining in xylem fluid and bound to CuO NPs after 3 h incubation by lithium dodecyl sulfate polyacrylamide gel electrophoresis (LDS-PAGE). After separating the CuO NP-bound proteins from those in solution by centrifugation, we fractionated the proteins in the supernatant and extracted from the pellet by LDS-PAGE and visualized the proteins by silver staining. Figure 7 shows an image of the resulting silver-stained gel which includes xylem fluid after exposure to 0 1000 mg·L⁻¹ CuO NPs (lanes 2, 3), and corona components extracted from the surface of the NPs (lanes 4, 5). The features in lane 4 (corresponding to proteins extracted pellets from the 0 mg·L⁻¹ CuO NP exposures) are too weak to reliably observe. Lanes 2 and 4 (supernatant and pellet from the 0 mg·L⁻¹ CuO NP exposure) demonstrate that the centrifugation procedure used does not lead to the sedimentation of detectable amounts of proteins in the absence of CuO NPs. The banding pattern produced by corona components extracted from the NPs after exposure to 1000 mg·L⁻¹ CuO NPs (lane 5) differs from that for the starting xylem fluid (lane 2). Specifically, the most intense bands in lane 5 correspond to a molecular mass of approximately 6 kDa, while that in lane 2 occurs at a molecular mass of approximately 9 kDa. Lane 2 contains multiple bands between 28 and 49 kDa, while lane 5 contains no observable bands in this region. This result indicates that the relative proportion of xylem fluid proteins in the extracted protein corona differs from that in the

xylem fluid; the most abundant proteins in the extracted corona do not correspond to the most abundant proteins in the xylem fluid.

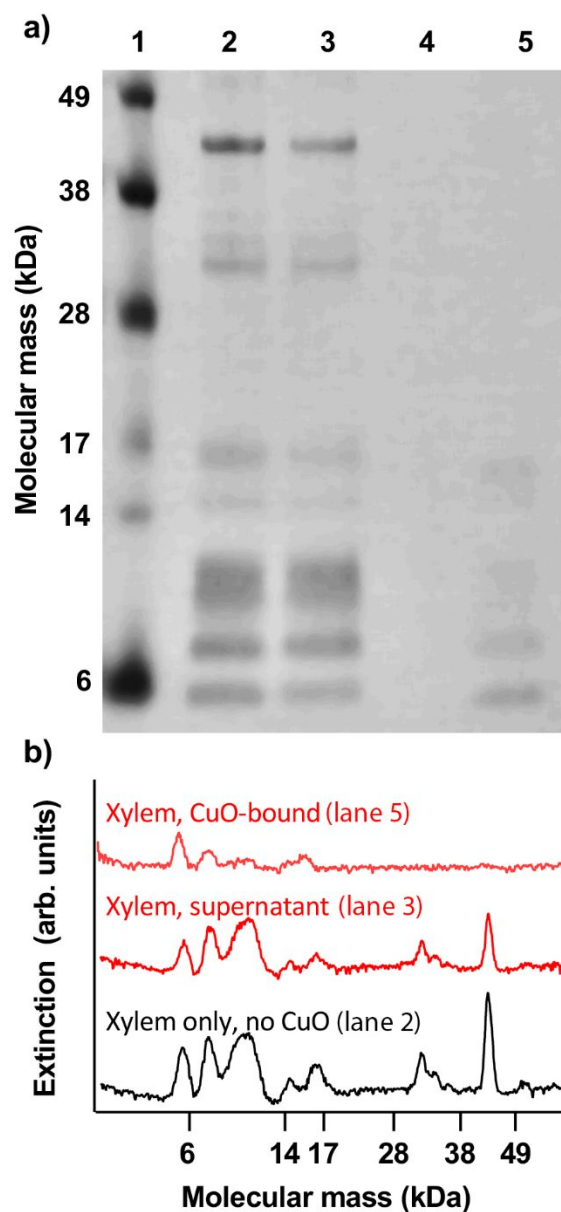


Figure 7. Protein binding to the CuO NPs was selective. (a) Proteins from xylem fluid before and after association with CuO NPs were fractionated by LDS-PAGE and visualized by silver staining: lane 1, molecular mass calibration standard; lanes 2, 3, supernatant after incubation with 0 and 1000 mg·L⁻¹ CuO NPs, respectively; lanes 4, 5, proteins extracted from NPs after incubation of xylem fluid with 0 and 1000 mg·L⁻¹ CuO NPs, respectively. (b) Extinction profiles showing intensity changes along lanes 2 and 3 (xylem fluid after incubation with 0 and 1000 mg·L⁻¹ CuO NPs, respectively) and lane 5 (proteins removed from 1000 mg·L⁻¹ CuO NP corona).

Corona formation dynamics

Previous studies in non-plant environments have shown that the corona evolves with time as layers formed initially under kinetic control are eventually (partially) replaced by more thermodynamically favored species.⁵⁵ To directly characterize the dynamic evolution of the corona and gain additional chemical information about the adsorbed layers, we used *in situ* ATR-FTIR spectroscopy in a flow cell geometry. We acquired FTIR spectra as a function of time during exposure to xylem as well as while rinsing to provide information about both the kinetics and reversibility of corona.

Figure 8 shows a spectrum of xylem fluid measured using ATR-FTIR using a trapezoidal ZnSe internal reflection element. The spectrum exhibits vibrational features typical of proteins.⁵⁶ These include a peak at 1636 cm^{-1} attributed to the peptide backbone Amide I band and the carboxylate asymmetric stretch; a peak 1541 cm^{-1} , consistent with the Amide II band, and a peak at 1231 cm^{-1} , consistent with the Amide III band.⁵⁷⁻⁵⁹ Peaks are also observed at 1394 cm^{-1} and 1348 cm^{-1} , which we attribute to COO^- symmetric stretch and the O–H deformation modes of carboxylic acids.⁶⁰ These carboxylic acid and carboxylate moieties may be attributed to small organic acids or the side chains of asparagine or glutamine residues in proteins or amino acids in xylem fluid.^{60, 61} Peaks at 1150 cm^{-1} and at 1081 cm^{-1} are consistent with C–O stretching modes associated with carbohydrates, or P–O–C stretching modes that may be associated with phospholipids, or C–OH modes associated with small carboxylic acids (Table S1). The peak near 1080 cm^{-1} is also consistent with spectra previously reported for carbohydrates and phospholipids.⁶²⁻⁶⁴ Prior studies have shown that xylem fluid from the members of the *Curcubita* genus contains proteins, carbohydrates, organic acids, and polyatomic ions such as ammonium and phosphate.^{31, 65-67} The infrared spectrum displayed in Fig. 8 indicates that proteins are present in the xylem fluid as well as phospholipids, carbohydrates, and/or carboxylate-containing molecules. Indexing the peaks in the xylem spectrum allows us to identify the biomolecules that bind to the surface of CuO NPs, and determine the dynamics of binding.

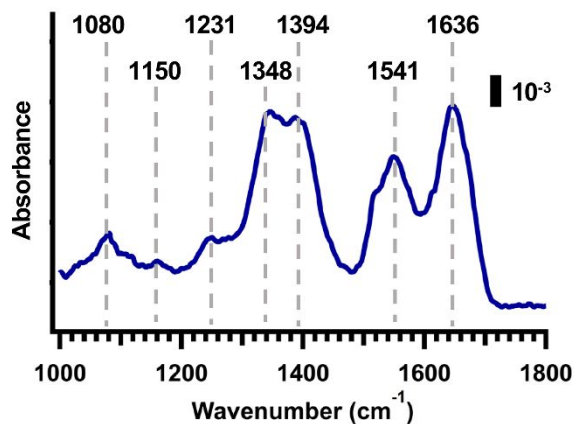


Figure 8. ATR-FTIR spectrum of xylem fluid. Peaks between 1700 and 1500 cm^{-1} reflect protein amide bonds or the presence of carboxylates. The peaks between 1450 and 1250 cm^{-1} indicate the presence of carboxylate moieties, that we attribute to small organic acids or the side chains of asparagine or glutamine residues in proteins or amino acids in xylem fluid. The peak between 1200 and 1000 cm^{-1} is likely due to the presence of carbohydrates.

Figure 9 shows FTIR spectra of xylem fluid interacting with CuO NPs for different time periods. To obtain these spectra we coated a Ge IRE with a thin, uniform layer of CuO NPs. We optimized the

1
2
3 preparation conditions and used scanning electron microscopy to verify complete, uniform coverage with
4 CuO NPs as demonstrated in the micrograph in Fig. S7. The CuO layer is sufficiently thin that the electric
5 field of the infrared light penetrates through the CuO layer. To collect *in situ* ATR-FTIR measurements a
6 reference spectrum was first collected of the CuO film in nanopure water. After the background scan was
7 collected, xylem fluid was flowed through the ATR cell and *in situ* FTIR spectra were collected
8 continuously; after 52 spectra were obtained (3. h) the sample was rinsed with water and additional
9 spectra were obtained. Figure 9 shows a representative FTIR spectra acquired at different time points.
10 Water gives rise to an asymmetric peak centered near 1638 cm^{-1} . The first spectrum measured after
11 introducing xylem ("S0", shown here magnified 10-fold) shows only a very weak water feature at 1638
12 cm^{-1} , that overlaps with the Amide I band peaking at 1636 cm^{-1} . Subsequent spectra S1, S5, S25, and S51
13 show new peaks with maxima near 1073 cm^{-1} , 1398 cm^{-1} , and 1562 cm^{-1} . Based on the analysis of pure
14 xylem fluid and spectra collected of model molecules (Figure 8, Figure S8), we attribute these peaks to
15 carbohydrates or phosphate containing molecules (1073 cm^{-1}), small molecules with carboxylate moieties
16 (1398 cm^{-1}), and proteins (1562 cm^{-1}). The absorbance of these three features increases with exposure
17 duration. To test the degree that molecular layer adsorption is reversible, we rinsed the sample for 3 h
18 with ultrapure water to remove weakly adsorbed molecules. Spectra S67 (approximately 1 h rinsing) and
19 S76 (approximately 1.5 h rinsing) show that the carbohydrate or phosphate containing molecule feature
20 at 1073.2 cm^{-1} is removed during rinsing while the vibrational features at 1398 cm^{-1} and 1562 cm^{-1} persist.
21 These results indicate that protein interacts more strongly with the CuO surface than do carbohydrates,
22 and protein binding is largely irreversible on the time-scale of our experiments; this implies that the XPS
23 data and BCA assays (which require a brief rinsing of the sample) are good probes of the protein
24 component of the coronas, but that more weakly adsorbed carbohydrates or phospholipids were rinsed
25 away during XPS and phenol assay sample preparation.
26
27
28
29
30
31
32
33
34
35
36
37
38
39
40
41
42
43
44
45
46
47
48
49
50
51
52
53
54
55
56
57
58
59
60

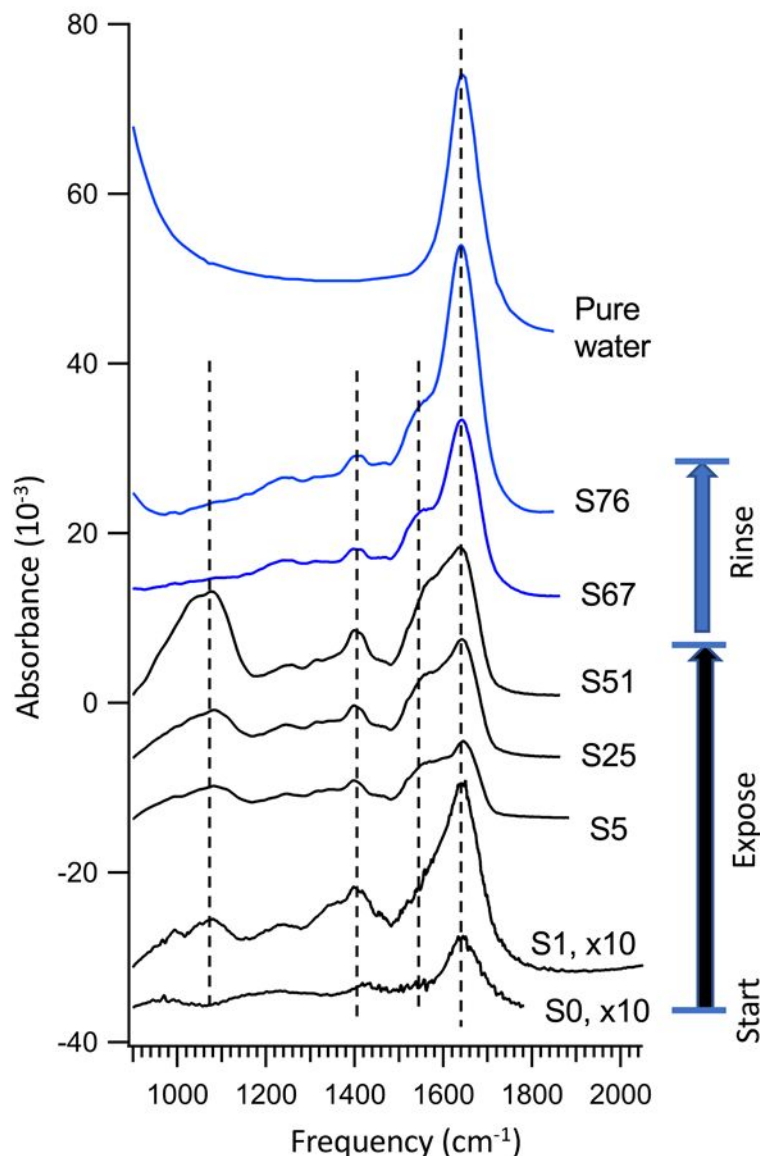


Figure 9. FTIR spectra of xylem fluid interacting with CuO-coated ZnSe as a function of exposure and rinsing time. The scans are identified by S#, where # is the number of scans that have been collected, with the label (S0, S1, etc.) representing the order in which the spectra were obtained; also shown is an absorption spectrum of pure water for reference.

Conclusion

Our results demonstrate that CuO NPs acquire a biomolecular corona from native pumpkin xylem fluid that contains both proteins and carbohydrates. Results from LDS-PAGE, ATR-FTIR, and XPS experiments show that the corona is composed primarily from proteins, despite the mass concentration of carbohydrates in xylem fluid being substantially higher than that of proteins. Furthermore, our results show that protein adsorption is *selective*; a subset of proteins having a molecular mass of approximately 6 kDa appear to be enriched in the corona relative to other xylem fluid proteins. Selectivity of protein binding is evidenced by the distribution of proteins extracted from the CuO NP surfaces differing from

1
2
3 that of the starting xylem fluid (Fig. 7) and by the decrease in average corona thickness from ~5.1 nm to
4 ~1.9 nm as the CuO NP concentration increases from 50 to 1000 mg L⁻¹, even though the total
5 concentration of protein in solution is reduced by only approximately 15% (Fig. 3b).
6

7 While quasi-irreversible binding of proteins to metal oxides has been reported previously, most
8 studies have primarily focused on isolated proteins or on corona formation in mammalian vasculature.^{68, 69}
9 In comparison, xylem fluid has a higher ratio of carbohydrates to proteins,^{31, 32} suggesting that
10 carbohydrates could play a more important role in corona formation in xylem fluid than in matrices
11 investigated previously. The high carbohydrate concentration in xylem is demonstrated in our own
12 measurements (Fig. 3) showing that the total mass concentration of carbohydrates is more than three
13 times that of proteins. The high concentration of carbohydrates in xylem fluid suggests that nanoparticle
14 coronas formed in plants could differ significantly from those formed in the mammalian serum and tissue.
15 Carbohydrates in xylem are present predominantly as oligosaccharides, with polysaccharides constituting
16 <5% of total carbohydrate mass.⁷⁰ While we have not investigated the distribution of carbohydrate masses
17 in the xylem fluid used here, our data show that carbohydrates in xylem fluid interact with CuO
18 nanoparticles, but that over time periods of minutes these carbohydrates are replaced by protein and can
19 be readily removed by simple water rinse. These observations indicate that even though carbohydrates
20 are present at higher concentrations than proteins in xylem, CuO nanoparticles exhibit a stronger affinity
21 for the amino acid residue side chains of proteins than for the sugar residues making up carbohydrate. As
22 a consequence, proteins dominate the corona composition formed in xylem. These observations are
23 consistent with past studies demonstrating low abundance of carbohydrates in nanoparticle coronas even
24 when abundant in the biological matrix.^{28, 71} We hypothesize that the higher affinity for amino acid side
25 chains likely arise from the presence of negatively charged functional groups on the proteins, driving an
26 electrostatic attraction to the positively charged CuO NP surface. Electrostatically driven binding is
27 consistent with the strong reduction in CuO NP electrophoretic mobility when suspended in xylem fluid.
28 Electrostatics has been previously reported to play an important role in corona acquisition from animal
29 and bacterial systems.⁷² We note that most metal oxide nanoparticles commonly investigated, including
30 TiO₂, Fe₂O₃, and SiO₂, often have negative zeta potential at circumneutral pH,⁷³ while that of the studied
31 CuO is positive. The nature of the protein corona is expected to depend on the sign and magnitude of
32 nanoparticle surface charge, such that coronas formed on CuO might be distinct from those formed on
33 many other metal oxides.
34

35 The acquisition of a biomolecular corona from xylem fluid may influence dissolution and
36 distribution of inorganic NPs in plants, as well as alter the available concentration of specific proteins
37 within the xylem fluid. We expect protein coronas to form on the surface of NPs in xylem fluid from a wide
38 range of plant species, as variation in xylem fluid composition is relatively small among plant species.^{33, 40}
39 However, we anticipate that the identity of biomolecules in the corona to be influenced by nanoparticle
40 surface charge, composition, and size.⁷⁴ In an agricultural or environmental setting, engineered
41 nanoparticles may encounter other complex media before entering xylem fluid. For instance,
42 nanoparticles that enter the plant *via* the root may have previously acquired corona that contains
43 components from soil organic matter, the soil microbiome, or root exudates. Particles on the leaf surface
44 interact with a hydrophobic interface populated by a diverse microbial community that may lead to
45 corona formation. Future studies to understand the effect of soil, root, phloem, and other extracellular
46 matrices on NP corona formation are needed to provide a more complete view of NP transformations
47
48
49
50
51
52
53
54
55
56
57
58
59
60

1
2
3 after environmental exposure, enable more accurate assessment of NP risk, and guide the tunable
4 synthesis of responsive materials as part of nano-enabled precision agriculture.
5

6 **Acknowledgments**

7
8 This material is based upon work supported by the National Science Foundation under Grant No. CHE-
9 2001611, the NSF Center for Sustainable Nanotechnology (CSN). The CSN is part of the Centers for
10 Chemical Innovation (CCI) Program.
11

12 **ORCID ID**

13
14 Robert J. Hamers 0000-0003-3821-9625

15 Joel A. Pedersen: 0000-0002-3918-1860

16 Christian A. Lochbaum: 0000-0002-1955-2118

17 Jason C. White: 0000-0001-5001-8143

18 Wade Elmer: 0000-0003-3308-4899

19 Jaya Borgatta: 0000-0002-9381-6097
20
21
22

23 **References**

- 24
25 1. M. Hadjidemetriou and K. Kostarelos, Nanomedicine: Evolution of the nanoparticle corona, *Nat*
26 *Nanotechnol*, 2017, **12**, 288-290.
27 2. M. P. Monopoli, C. Aberg, A. Salvati and K. A. Dawson, Biomolecular coronas provide the biological
28 identity of nanosized materials, *Nat Nanotechnol*, 2012, **7**, 779-786.
29 3. D. Docter, D. Westmeier, M. Markiewicz, S. Stolte, S. Knauer and R. Stauber, The nanoparticle
30 biomolecule corona: lessons learned—challenge accepted?, *Chemical Society Reviews*, 2015, **44**,
31 6094-6121.
32 4. A. Albanese, C. D. Walkey, J. B. Olsen, H. Guo, A. Emili and W. C. Chan, Secreted biomolecules alter
33 the biological identity and cellular interactions of nanoparticles, *ACS Nano*, 2014, **8**, 5515-5526.
34 5. V. Francia, K. Yang, S. Deville, C. Reker-Smit, I. Nelissen and A. Salvati, Corona Composition Can
35 Affect the Mechanisms Cells Use to Internalize Nanoparticles, *ACS Nano*, 2019, **13**, 11107-11121.
36 6. G. Caracciolo, S. Palchetti, V. Colapicchioni, L. Digiacomio, D. Pozzi, A. L. Capriotti, G. La Barbera
37 and A. Lagana, Stealth effect of biomolecular corona on nanoparticle uptake by immune cells,
38 *Langmuir*, 2015, **31**, 10764-10773.
39 7. M. N. Gupta and I. Roy, How Corona Formation Impacts Nanomaterials as Drug Carriers, *Mol*
40 *Pharm*, 2020, **17**, 725-737.
41 8. Y. Yue, R. Behra, L. Sigg, M. J. F. Suter, S. Pillai and K. Schirmer, Silver nanoparticle–protein
42 interactions in intact rainbow trout gill cells, *Environmental Science: Nano*, 2016, **3**, 1174-1185.
43 9. G. Maiorano, S. Sabella, B. Sorce, V. Brunetti, M. A. Malvindi, R. Cingolani and P. P. Pompa, Effects
44 of cell culture media on the dynamic formation of protein-nanoparticle complexes and influence
45 on the cellular response, *ACS Nano*, 2010, **4**, 7481-7491.
46 10. S. Tenzer, D. Docter, S. Rosfa, A. Wlodarski, J. Kuharev, A. Rekić, S. K. Knauer, C. Bantz, T. Nawroth,
47 C. Bier, J. Sirirattanapan, W. Mann, L. Treuel, R. Zellner, M. Maskos, H. Schild and R. H. Stauber,
48 Nanoparticle size is a critical physicochemical determinant of the human blood plasma corona: a
49 comprehensive quantitative proteomic analysis, *ACS Nano*, 2011, **5**, 7155-7167.
50 11. C. Gunawan, M. Lim, C. P. Marquis and R. Amal, Nanoparticle-protein corona complexes govern
51 the biological fates and functions of nanoparticles, *J Mater Chem B*, 2014, **2**, 2060-2083.
52
53
54
55
56
57
58
59
60

12. J. Borgatta, C. Ma, N. Hudson-Smith, W. Elmer, C. D. Plaza Pérez, R. De La Torre-Roche, N. Zuverza-Mena, C. L. Haynes, J. C. White and R. J. Hamers, Copper Based Nanomaterials Suppress Root Fungal Disease in Watermelon (*Citrullus lanatus*): Role of Particle Morphology, Composition and Dissolution Behavior, *ACS Sustainable Chemistry & Engineering*, 2018, **6**, 14847-14856.
13. W. Elmer, R. De La Torre-Roche, L. Pagano, S. Majumdar, N. Zuverza-Mena, C. Dimkpa, J. Gardea-Torresdey and J. C. White, Effect of Metalloid and Metal Oxide Nanoparticles on Fusarium Wilt of Watermelon, *Plant Dis*, 2018, **102**, 1394-1401.
14. C. D. P. Perez, R. De La Torre Roche, N. Zuverza-Mena, C. Ma, Y. Shen, J. C. White, E. A. Pozza, A. A. Pozza and W. H. Elmer, Metalloid and Metal Oxide Nanoparticles Suppress Sudden Death Syndrome of Soybean, *J Agric Food Chem*, 2020, **68**, 77-87.
15. C. Ma, J. Borgatta, R. De La Torre-Roche, N. Zuverza-Mena, J. C. White, R. J. Hamers and W. H. Elmer, Time-dependent transcriptional response of tomato (*Solanum lycopersicum* L.) to Cu nanoparticle exposure upon infection with *Fusarium oxysporum* f. sp. *lycopersici*, *ACS Sustainable Chemistry & Engineering*, 2019, **7**, 10064-10074.
16. C. Ma, J. Borgatta, B. G. Hudson, A. A. Tamijani, R. De La Torre-Roche, N. Zuverza-Mena, Y. Shen, W. Elmer, B. Xing, S. E. Mason, R. J. Hamers and J. C. White, Advanced material modulation of nutritional and phytohormone status alleviates damage from soybean sudden death syndrome, *Nat Nanotechnol*, 2020, **15**, 1033-1042.
17. Y. Shen, J. Borgatta, C. Ma, W. Elmer, R. J. Hamers and J. C. White, Copper Nanomaterial Morphology and Composition Control Foliar Transfer through the Cuticle and Mediate Resistance to Root Fungal Disease in Tomato (*Solanum lycopersicum*), *J Agric Food Chem*, 2020, **68**, 11327-11338.
18. T. Hofmann, G. V. Lowry, S. Ghoshal, N. Tufenkji, D. Brambilla, J. R. Dutcher, L. M. Gilbertson, J. P. Giraldo, J. M. Kinsella and M. P. Landry, Technology readiness and overcoming barriers to sustainably implement nanotechnology-enabled plant agriculture, *Nature Food*, 2020, **1**, 416-425.
19. Z. Wang, X. Xie, J. Zhao, X. Liu, W. Feng, J. C. White and B. Xing, Xylem- and phloem-based transport of CuO nanoparticles in maize (*Zea mays* L.), *Environmental science & technology*, 2012, **46**, 4434-4441.
20. J. Kurepa, T. E. Shull and J. A. Smalle, Metabolomic analyses of the bio-corona formed on TiO₂ nanoparticles incubated with plant leaf tissues, *J Nanobiotechnology*, 2020, **18**, 28.
21. S. Prakash and R. Deswal, Analysis of temporally evolved nanoparticle-protein corona highlighted the potential ability of gold nanoparticles to stably interact with proteins and influence the major biochemical pathways in *Brassica juncea*, *Plant Physiol Biochem*, 2020, **146**, 143-156.
22. E. Spielman-Sun, A. Avellan, G. D. Bland, R. V. Tappero, A. S. Acerbo, J. M. Unrine, J. P. Giraldo and G. V. Lowry, Nanoparticle surface charge influences translocation and leaf distribution in vascular plants with contrasting anatomy, *Environmental Science: Nano*, 2019, **6**, 2508-2519.
23. A. Avellan, J. Yun, Y. Zhang, E. Spielman-Sun, J. M. Unrine, J. Thieme, J. Li, E. Lombi, G. Bland and G. V. Lowry, Nanoparticle Size and Coating Chemistry Control Foliar Uptake Pathways, Translocation, and Leaf-to-Rhizosphere Transport in Wheat, *ACS Nano*, 2019, **13**, 5291-5305.
24. E. Spielman-Sun, E. Lombi, E. Donner, A. Avellan, B. Etschmann, D. Howard and G. V. Lowry, Temporal Evolution of Copper Distribution and Speciation in Roots of *Triticum aestivum* Exposed to CuO, Cu(OH)₂, and CuS Nanoparticles, *Environ Sci Technol*, 2018, **52**, 9777-9784.
25. E. Spielman-Sun, E. Lombi, E. Donner, D. Howard, J. M. Unrine and G. V. Lowry, Impact of Surface Charge on Cerium Oxide Nanoparticle Uptake and Translocation by Wheat (*Triticum aestivum*), *Environ Sci Technol*, 2017, **51**, 7361-7368.
26. Y. Su, V. Ashworth, C. Kim, A. S. Adeleye, P. Rolshausen, C. Roper, J. White and D. Jassby, Delivery, uptake, fate, and transport of engineered nanoparticles in plants: a critical review and data analysis, *Environmental Science: Nano*, 2019, **6**, 2311-2331.

- 1
- 2
- 3
- 4 27. M. Lundqvist, J. Stigler, G. Elia, I. Lynch, T. Cedervall and K. A. Dawson, Nanoparticle size and
- 5 surface properties determine the protein corona with possible implications for biological impacts,
- 6 *Proc Natl Acad Sci U S A*, 2008, **105**, 14265-14270.
- 7 28. K. Grintzalis, T. N. Lawson, F. Nasser, I. Lynch and M. R. Viant, Metabolomic method to detect a
- 8 metabolite corona on amino-functionalized polystyrene nanoparticles, *Nanotoxicology*, 2019, **13**,
- 9 783-794.
- 10 29. A. C. Mensch, R. T. Hernandez, J. E. Kuether, M. D. Torelli, Z. V. Feng, R. J. Hamers and J. A.
- 11 Pedersen, Natural Organic Matter Concentration Impacts the Interaction of Functionalized
- 12 Diamond Nanoparticles with Model and Actual Bacterial Membranes, *Environ Sci Technol*, 2017,
- 13 **51**, 11075-11084.
- 14 30. M. Pink, N. Verma, C. Kersch and S. Schmitz-Spanke, Identification and characterization of small
- 15 organic compounds within the corona formed around engineered nanoparticles, *Environmental*
- 16 *Science: Nano*, 2018, **5**, 1420-1427.
- 17 31. S. Satoh, C. Iizuka, A. Kikuchi, N. Nakamura and T. Fujii, Proteins and carbohydrates in xylem sap
- 18 from squash root, *Plant and cell physiology*, 1992, **33**, 841-847.
- 19 32. M. van Helden, W. F. Tjallingh and T. A. van Beek, Phloem sap collection from lettuce (*Lactuca*
- 20 *sativa* L.): chemical comparison among collection methods, *Journal of Chemical Ecology*, 1994, **20**,
- 21 3191-3206.
- 22 33. A. Buhtz, A. Kolasa, K. Arlt, C. Walz and J. Kehr, Xylem sap protein composition is conserved among
- 23 different plant species, *Planta*, 2004, **219**, 610-618.
- 24 34. J. L. Dacheux, C. Belleannee, R. Jones, V. Labas, M. Belghazi, B. Guyonnet, X. Druart, J. L. Gatti and
- 25 F. Dacheux, Mammalian epididymal proteome, *Mol Cell Endocrinol*, 2009, **306**, 45-50.
- 26 35. L. Zhao, C. Ortiz, A. S. Adeleye, Q. Hu, H. Zhou, Y. Huang and A. A. Keller, Metabolomics to Detect
- 27 Response of Lettuce (*Lactuca sativa*) to Cu(OH)₂ Nanopesticides: Oxidative Stress Response and
- 28 Detoxification Mechanisms, *Environ Sci Technol*, 2016, **50**, 9697-9707.
- 29 36. G. W. Koch and A. L. Fredeen, in *Vascular Transport in Plants*, eds. N. M. Holbrook and M. A.
- 30 Zwieniecki, Academic Press, Burlington, 2005, DOI: 10.1016/b978-012088457-5/50023-x, pp. 437-
- 31 456.
- 32 37. M. Dubois, K. A. Gilles, J. K. Hamilton, P. t. Rebers and F. Smith, Colorimetric method for
- 33 determination of sugars and related substances, *Analytical chemistry*, 1956, **28**, 350-356.
- 34 38. S. Åsbrink and L.-J. Norrby, A refinement of the crystal structure of copper (II) oxide with a
- 35 discussion of some exceptional esd's, *Acta Crystallographica Section B: Structural Crystallography*
- 36 *and Crystal Chemistry*, 1970, **26**, 8-15.
- 37 39. D. Su, X. Xie, S. Dou and G. Wang, CuO single crystal with exposed {001} facets--a highly efficient
- 38 material for gas sensing and Li-ion battery applications, *Sci Rep*, 2014, **4**, 5753.
- 39 40. A. D. Peuke, Correlations in concentrations, xylem and phloem flows, and partitioning of elements
- 40 and ions in intact plants. A summary and statistical re-evaluation of modelling experiments in
- 41 *Ricinus communis*, *J Exp Bot*, 2010, **61**, 635-655.
- 42 41. T. Oncsik, G. Trefalt, M. Borkovec and I. Szilagy, Specific ion effects on particle aggregation
- 43 induced by monovalent salts within the Hofmeister series, *Langmuir*, 2015, **31**, 3799-3807.
- 44 42. J. Chorover, Comparison of Hematite Coagulation by Charge Screening and Phosphate Adsorption:
- 45 Differences in Aggregate Structure, *Clays and Clay Minerals*, 1997, **45**, 690-708.
- 46 43. T. A. Oleson and N. Sahaj, Interaction energies between oxide surfaces and multiple
- 47 phosphatidylcholine bilayers from extended-DLVO theory, *J Colloid Interface Sci*, 2010, **352**, 316-
- 48 326.
- 49 44. P. Richardson, D. Baker and L. Ho, The chemical composition of cucurbit vascular exudates, *Journal*
- 50 *of experimental Botany*, 1982, **33**, 1239-1247.
- 51
- 52
- 53
- 54
- 55
- 56
- 57
- 58
- 59
- 60

- 1
- 2
- 3
- 4 45. H. Fischer, I. Polikarpov and A. F. Craievich, Average protein density is a molecular-weight-
- 5 dependent function, *Protein Sci*, 2004, **13**, 2825-2828.
- 6 46. C.-K. Wu, M. Yin, S. O'Brien and J. T. Koberstein, Quantitative Analysis of Copper Oxide
- 7 Nanoparticle Composition and Structure by X-ray Photoelectron Spectroscopy, *Chemistry of*
- 8 *Materials*, 2006, **18**, 6054-6058.
- 9 47. J.-C. Dupin, D. Gonbeau, P. Vinatier and A. Levasseur, Systematic XPS studies of metal oxides,
- 10 hydroxides and peroxides, *Physical Chemistry Chemical Physics*, 2000, **2**, 1319-1324.
- 11 48. M. H. Ahmed, J. A. Byrne, J. McLaughlin and W. Ahmed, Study of human serum albumin adsorption
- 12 and conformational change on DLC and silicon doped DLC using XPS and FTIR spectroscopy, 2013.
- 13 49. C. Stavis, T. L. Clare, J. E. Butler, A. D. Radadia, R. Carr, H. Zeng, W. P. King, J. A. Carlisle, A.
- 14 Aksimentiev, R. Bashir and R. J. Hamers, Surface functionalization of thin-film diamond for highly
- 15 stable and selective biological interfaces, *Proc Natl Acad Sci U S A*, 2011, **108**, 983-988.
- 16 50. S. Ray and A. G. Shard, Quantitative analysis of adsorbed proteins by X-ray photoelectron
- 17 spectroscopy, *Anal Chem*, 2011, **83**, 8659-8666.
- 18 51. T. L. Clare, B. H. Clare, B. M. Nichols, N. L. Abbott and R. J. Hamers, Functional monolayers for
- 19 improved resistance to protein adsorption: oligo(ethylene glycol)-modified silicon and diamond
- 20 surfaces, *Langmuir*, 2005, **21**, 6344-6355.
- 21 52. E. Vanea and V. Simon, XPS study of protein adsorption onto nanocrystalline aluminosilicate
- 22 microparticles, *Applied Surface Science*, 2011, **257**, 2346-2352.
- 23 53. P. Guerrero, T. Garrido, I. Leceta and K. de la Caba, Films based on proteins and polysaccharides:
- 24 Preparation and physical-chemical characterization, *European Polymer Journal*, 2013, **49**, 3713-
- 25 3721.
- 26 54. K. E. Dombrowski, S. E. Wright, J. C. Birkbeck and W. E. Moddeman, in *Methods in Protein Structure*
- 27 *Analysis*, Springer, 1995, pp. 251-260.
- 28 55. D. Docter, U. Distler, W. Storck, J. Kuharev, D. Wünsch, A. Hahlbrock, S. K. Knauer, S. Tenzer and
- 29 R. H. Stauber, Quantitative profiling of the protein coronas that form around nanoparticles,
- 30 *Nature Protocols*, 2014, **9**, 2030.
- 31 56. A. Barth and C. Zscherp, What vibrations tell about proteins, *Quarterly reviews of biophysics*, 2002,
- 32 **35**, 369-430.
- 33 57. U. Bocker, S. G. Wubshet, D. Lindberg and N. K. Afseth, Fourier-transform infrared spectroscopy
- 34 for characterization of protein chain reductions in enzymatic reactions, *Analyt*, 2017, **142**, 2812-
- 35 2818.
- 36 58. K. K. Chittur, FTIR/ATR for protein adsorption to biomaterial surfaces, *Biomaterials*, 1998, **19**, 357-
- 37 369.
- 38 59. P. I. Haris and F. Severcan, FTIR spectroscopic characterization of protein structure in aqueous and
- 39 non-aqueous media, *Journal of Molecular Catalysis B: Enzymatic*, 1999, **7**, 207-221.
- 40 60. A. Barth, Infrared spectroscopy of proteins, *Biochim Biophys Acta*, 2007, **1767**, 1073-1101.
- 41 61. R. Rellan-Alvarez, H. El-Jendoubi, G. Wohlgemuth, A. Abadia, O. Fiehn, J. Abadia and A. Alvarez-
- 42 Fernandez, Metabolite profile changes in xylem sap and leaf extracts of strategy I plants in
- 43 response to iron deficiency and resupply, *Front Plant Sci*, 2011, **2**, 66.
- 44 62. C. Zhou, W. Jiang, B. K. Via, O. Fasina and G. Han, Prediction of mixed hardwood lignin and
- 45 carbohydrate content using ATR-FTIR and FT-NIR, *Carbohydr Polym*, 2015, **121**, 336-341.
- 46 63. J. K. Kumar and A. D. Prasad, Identification and comparison of biomolecules in medicinal plants of
- 47 Tephrosia tinctoria and Atylosia albicans by using FTIR, *Rom. J. Biophys*, 2011, **21**, 63-71.
- 48 64. J. Nzai and A. Proctor, Determination of phospholipids in vegetable oil by Fourier transform
- 49 infrared spectroscopy, *Journal of the American Oil Chemists' Society*, 1998, **75**, 1281-1289.
- 50 65. E. Tatár, V. G. Mihucz, A. Varga, G. Záray and F. Fodor, Determination of Organic Acids in Xylem
- 51 Sap of Cucumber: Effect of Lead Contamination, *Microchemical Journal*, 1998, **58**, 306-314.
- 52
- 53
- 54
- 55
- 56
- 57
- 58
- 59
- 60

- 1
2
3 66. R. S. Harrison-Murray and D. T. Clarkson, Relationships between structural development and the
4 absorption of ions by the root system of *Cucurbita pepo*, *Planta*, 1973, **114**, 1-16.
5
6 67. J. Rodríguez-Celma, L. Ceballos-Laita, M. A. Grusak, J. Abadía and A.-F. López-Millán, Plant fluid
7 proteomics: delving into the xylem sap, phloem sap and apoplastic fluid proteomes, *Biochimica*
8 *et Biophysica Acta (BBA)-Proteins and Proteomics*, 2016, **1864**, 991-1002.
9
10 68. S. Wan, P. M. Kelly, E. Mahon, H. Stockmann, P. M. Rudd, F. Caruso, K. A. Dawson, Y. Yan and M.
11 P. Monopoli, The "sweet" side of the protein corona: effects of glycosylation on nanoparticle-cell
12 interactions, *ACS Nano*, 2015, **9**, 2157-2166.
13
14 69. Z. J. Deng, G. Mortimer, T. Schiller, A. Musumeci, D. Martin and R. F. Minchin, Differential plasma
15 protein binding to metal oxide nanoparticles, *Nanotechnology*, 2009, **20**, 455101.
16
17 70. H. Iwai, M. Usui, H. Hoshino, H. Kamada, T. Matsunaga, K. Kakegawa, T. Ishii and S. Satoh, Analysis
18 of sugars in squash xylem sap, *Plant Cell Physiol*, 2003, **44**, 582-587.
19
20 71. M. Baalousha, K. Afshinnia and L. Guo, Natural organic matter composition determines the
21 molecular nature of silver nanomaterial-NOM corona, *Environmental Science: Nano*, 2018, **5**, 868-
22 881.
23
24 72. K. P. García, K. Zarschler, L. Barbaro, J. A. Barreto, W. O'Malley, L. Spiccia, H. Stephan and B.
25 Graham, Zwitterionic-coated "stealth" nanoparticles for biomedical applications: recent advances
26 in countering biomolecular corona formation and uptake by the mononuclear phagocyte system,
27 *Small*, 2014, **10**, 2516-2529.
28
29 73. Y. Zhang, Y. Chen, P. Westerhoff and J. Crittenden, Impact of natural organic matter and divalent
30 cations on the stability of aqueous nanoparticles, *Water Res*, 2009, **43**, 4249-4257.
31
32 74. A. Albanese, P. S. Tang and W. C. W. Chan, in *Annual Review of Biomedical Engineering, Vol 14*,
33 ed. M. L. Yarmush, Annual Reviews, Palo Alto, 2012, vol. 14, pp. 1-16.
34
35
36
37
38
39
40
41
42
43
44
45
46
47
48
49
50
51
52
53
54
55
56
57
58
59
60